Complex electric fields near the lunar terminator: The near-surface wake and accelerated dust

W. M. Farrell,[1] T. J. Stubbs,[2,3] R. R. Vondrak,[1] G. T. Delory,[4] and J. S. Halekas[4]

Received 10 January 2007; revised 27 April 2007; accepted 16 May 2007; published 18 July 2007.

[1] The lunar near-surface electric field in the vicinity of the terminator is very complex, with a surface polarity change from dayside-positive to nightside-negative potentials and the formation of intensely negative potentials due to the low plasma density and increased temperatures in the trailing lunar wake region. Presented is a preliminary map of the terminator near-surface E-field magnitude and a discussion of dust dynamics in this E-field structure, with intense vertical fields tending to give rise to vertically directed dust trajectories (aligned with the surface normal). Application of this process of wake-generated surface E-fields and dust to the more complicated topography at the lunar landing site of Apollo 17 is then used to explain the detection of fast moving (~500 m/sec) but nightside-directed dust in the region. We suggest that local solar wind orographic effects occurring at lunar sunrise/sunset can create a plasma void on the anti-sunward side of obstructing features and associated wake-generated surface E-fields can then be the source of the nightside-directed grains. **Citation:** Farrell, W. M., T. J. Stubbs, R. R. Vondrak, G. T. Delory, and J. S. Halekas (2007), Complex electric fields near the lunar terminator: The near-surface wake and accelerated dust, *Geophys. Res. Lett.*, *34*, L14201, doi:10.1029/2007GL029312.

1. Introduction

[2] The Moon is often considered to be a static environment. However, Apollo observations [*McCoy and Criswell*, 1974; *Berg et al.*, 1976] and recent modeling [*Stubbs et al.*, 2006] suggest that the lunar regolith is in fact very active, creating a dynamic dusty exosphere that extends to altitudes in excess of 100 km. The forces that lift the charged dust are straightforward: on the lunar dayside, relatively strong photoemission currents render the surface positive with a potential of 1–5 V, and dust grains that are also photoemission-charged positive are lofted vertically via the repulsive near-surface forces. On the nightside, low density electron plasma currents render the surface a negative potential, and dust grains that are also plasma-charged negative are lofted vertically via repulsive forces. However, the most complicated electrical region on this solid body is near the terminator, where there is a distinct transition from sunlight-driven positive to plasma-created negative surface potential. Further complicating the situation is the formation of the lunar plasma wake in the solar wind created immediately nightside of the terminator [*Ogilvie et al.*, 1996; *Farrell et al.*, 1998; *Halekas et al.*, 2005] that progressively reduces the surface plasma density and increases surface electron temperature from the terminator to the anti-solar point, thereby creating very strong negative surface potentials. *Berg et al.* [1976] reported the detection of near-surface dust grains accelerated to > 0.5 km/sec in nightside regions at and behind the terminator. In this work, we will present a model of E-fields and show dust grain movement in the complex near-terminator lunar surface dusty-plasma environment.

[3] There is substantial evidence for an active lunar dusty exosphere. First, Apollo astronauts in orbit about the Moon reported the presence of a horizon glow and "streamers" just prior to sunrise. This glow is believed to be scattered light from high-altitude (~100 km) dust [*McCoy and Criswell*, 1974] lifted from the surface via a "dynamic dust fountain" effect recently modeled by *Stubbs et al.* [2006]. Second, GSFC's Lunar Ejecta and Meteorites (LEAM) surface instrument (deployed on the Moon during the Apollo 17 mission) detected highly accelerated dust twice per lunation peaking in activity when the sensors were located at the terminators [*Berg et al.*, 1976]. The events were more frequently observed at the sunrise terminator, with grain velocity components at both terminators predominately directed toward the nightside (anti-sunward grain flow), suggesting some systematic process is present at both terminators. To date, a nightside-directed dust acceleration mechanism has not been uniquely identified. In this work, we will examine the complex E-field near the terminator to derive a first-ever electrostatic mapping of the region with an objective to understand how dust grains get accelerated in these fields.

2. Surface Charging and the Lunar Wake

[4] The formalism to describe lunar surface charging is presented by *Manka* [1973], and we simply review the most critical elements of that work herein. The lunar surface will charge in an attempt to keep current balance. On the lunar dayside, photoemission currents, J_p, dominate at levels near 4 $\mu A/m^2$ at the subsolar point. With the loss of electrons, the surface tends to charge a few volts positive according the expression $e\varphi = kT_p \ln(J_p/J_e)$, where $k\ T_p/e$ is a nominal temperature for the photo-emitted electrons of 1–2 eV [*Manka*, 1973], J_p is the photoemission current and J_e is the plasma electron current. On the lunar nightside that faces the wake in the solar wind, the diminished electron

[1] Solar System Exploration Division, NASA Goddard Space Flight Center, Greenbelt, Maryland, USA.
[2] Goddard Earth Sciences and Technology Center, University of Maryland Baltimore County, Baltimore, Maryland, USA.
[3] Heliophysics Division, NASA Goddard Space Flight Center, Greenbelt, Maryland, USA.
[4] Space Science Laboratory, University of California, Berkeley, California, USA.

flux near the surface, J_e, typically dominates the ion flux, J_i, and hence the surface will charge negative according to the expression $e\varphi = -kT_e \ln(J_e/J_i)$, where k T_e/e is the electron temperature in units of electron-volts. The potential at point z located above the surface is $\varphi(z) = \varphi_o \exp(-z/\lambda_D)$, where λ_D is the plasma Debye length. The vertical electric field then becomes $E_z(z) = \varphi(z)/\lambda_D$ and the horizontal electric field is $E_\rho(z) = d\phi/d\rho$ where ρ is the coordinate tangent to the surface. In the typical solar wind, $n_e \sim n_i \sim$ 5 particles/cm^3, and $kT_e/e = kT_i/e \sim 10$ eV. Near the subsolar point, the ratio of photoemission-to-solar wind electron currents is $J_p/J_e \sim 10$.

[5] In the typical solar wind, the ratio of J_e/J_i is approximately constant. However, behind the terminator, the ratio of J_e/J_i does not stay constant, becoming progressively larger with surface distance from the terminator. This increase is due to the effects of the lunar wake. The solar wind flowing by the Moon is supersonic and nominally at about 400 km/sec. However, the plasma incident on the lunar dayside is absorbed creating a plasma void on the nightside, with observed geometrically decreasing plasma density and increasing electron temperature [*Ogilvie et al.*, 1996]. In a fluid (neutral) plasma perspective, *Samir et al.* [1983] suggested that a Maxwellian plasma void fills-in isothermally via a self-similar solution where the plasma density exponentially decreases with distance from the wake flank as $n_e = n_i = n_o \exp(-(Z/C_s + 1))$, with Z = s/t, s being the distance from the wake flank, t being the time after the creation of the void and C_s being the ion sound speed ($\sim$30 km/sec in the solar wind). In a time-stationary situation (steady solar wind flow), the wake evolution time, t, is also the convection time of a solar wind fluid element moving downstream (in the x direction) from the terminator, $t = x/V_{sw}$, where V_{sw} is the solar wind flow speed [see *Farrell et al.*, 1998, Figure 1]. Hence, $Z = (s/x)\, V_{sw}$ and $n_e = n_i = n_o \exp(-(sV_{sw}/xC_s + 1))$. *Halekas et al.* [2005] rederived the self-similar solution using kappa functions and found a similar geometric-like decrease in plasma density and linear-like increase in electron temperature with distance from the wake flank. *Halekas et al.* [2005] found $n_e = n_o\,(1 + AB)^{(1-2\kappa)}$ and $T_e = T_o\,(1 + AB)^2$ where $A = (2\kappa - 1)^{1/2}\,(2\kappa - 3)^{-1/2}\,(2\kappa - 2)^{-1}$, $B = Z/C_s + 1$ and κ is the value describing the kappa distribution ($\kappa \sim 4$). Deep in the central wake, T_e can become 6–10 times that of the nominal solar wind. Because of the increase in T_e, and the subsequent larger ratio of J_e/J_i, the surface potential can become very large & negative in the nightside lunar wake region [*Halekas et al.*, 2005; *Stubbs et al.*, 2007].

[6] *Manka* [1973] modeled the lunar surface potential up to and slightly past the terminator, but did not include nightside wake effects. We now augment that model by providing the low density and temperature variation associated with the nightside wake region to the surface potential calculation. In essence, we merge n and T of *Halekas et al.* [2005] with *Manka*'s [1973] formalism.

3. Model Results

[7] Figure 1 shows the modeled near-surface electric field magnitude, surface potential, plasma density and temperature (above the plasma sheath), and surface vertical and horizontal E-fields as a function of angle from the subsolar point using the potential expressions derivable from *Manka* [1973] and now incorporating the wake formalism for the kappa distributions described by *Halekas et al.* [2005]. In the nightside region where kappa solar wind distributions dominate, a new kappa current balance surface potential equation was applied in the form $e\varphi_n = kT_e\,(\kappa - 3/2)\,[1 - (J_e/J_i)^{-1/(1/2-\kappa)}]$. The solar wind density is assumed to be 5 particles/cm^3 and the solar wind electron and ion temperatures are assumed to be $\sim$10 eV. As indicated in Figures 1c and 1d, the near-surface electron density drops significantly (orders of magnitude) and electron temperature increases substantially in the wake region. The wake temperature increase is associated with the fastest electrons (at the tail of the solar wind electron thermal distribution) moving into the wake ahead of the slower electrons closer to the thermal core.

[8] Figure 1a shows a map of the E-field magnitude up to a height of 100-m. The "dead zone" labeled on Figure 1a is the location where the surface potential is zero (Figure 1b) and hence there is no vertical E-field (Figure 1e). As indicated by *Stubbs et al.* [2006], at this location there is no lofted dust since there is no vertical repulsive electric force to drive the lofting. This location corresponds to the transition at the surface from a photoelectron sheath (electrons emitted from surface) to a solar-wind plasma sheath (electrons collected at surface). As a consequence, the surface potential (Figure 1b) and vertical E-field (Figure 1e) makes a transition from positive to negative values. This transition does not occur exactly at the terminator, but at a subsolar angle of about 67°. This location is where the angle of solar incidence reduces the outward-directed photoemissive electron flux to approximately balance the inward-directed solar wind electron flux. Variations in solar wind electron current will change the latitude location of this current balance, thereby shifting the location of the deadzone.

[9] Figure 1b shows the surface potential as a function of subsolar angle. The structure of the potential up to 90° looks very similar to *Manka*'s [1973, Figure 1] with surface potentials going from values of a few volts positive on the dayside to −40 V at the terminator. However, *Manka* [1973] did not include effects from the wake at angles greater than 90°, like those incorporated here. We extend the earlier results by including the exponential loss of plasma (Figure 1c) and increase in electron temperature (Figure 1d) associated with the fluid wake equation as defined by *Halekas et al.* [2005]. Figure 1c indicates that the wake does not commence exactly at 90°, but extends about 7° into the dayside region with the presence of a rarefaction region typically found to extend outward from plasma wakes [*Samir et al.*, 1983; *Farrell et al.*, 1998]. The rarefaction region is a mathematical consequence of using the self-similar model, but its exact nature is unknown: There may simply be no rarefaction region and a discontinuity at the surface at 90°. However, such a discontinuity would be naturally unstable, giving rise to wave turbulence with modes having group velocities that allow wave propagation to extend upstream. The rarefaction wave may appear as a plasma ion sonic disturbance [*Ogilvie et al.*, 1996; *Farrell et al.*, 1998], and hence the primary wave mode may be ion sonic waves that act to transform the boundary from a sharp-varying transition to a more turbulent feature. Such kinetic turbulence is beyond the scope of the fluid model herein, and is clearly a topic for future study.

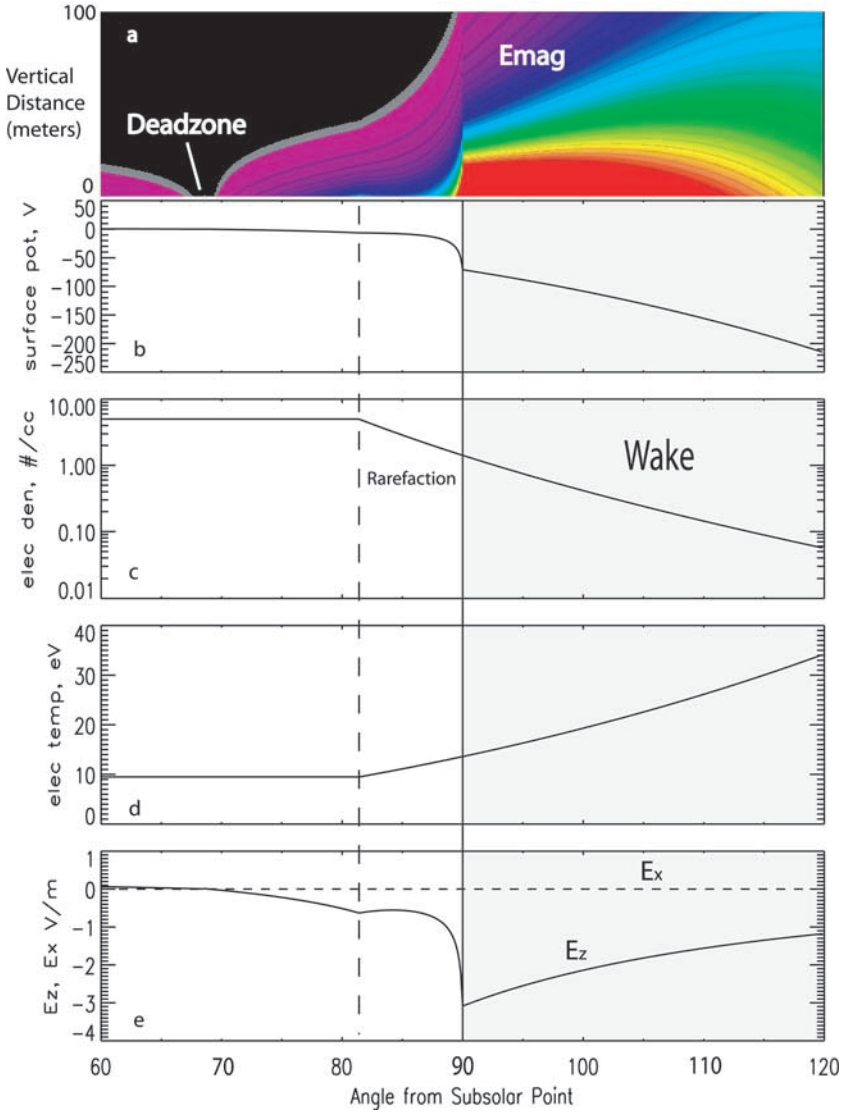

Figure 1. A model of the terminator (a) near-surface (<100 m) E-field magnitude, (b) surface potential, (c) solar wind electron density, (d) solar wind electron temperature, and (e) vertical (continuous line) and horizontal (dotted line) E-fields as a function of angle from the subsolar point. In Figure 1a, the color red indicates $|E| > 1.5$ V/m and black indicates $|E| = 0$ V/m.

[10] In Figures 1a and 1e, the E-fields reach a maximum near the terminator at about −3 V/m with the region of anomalously large E-fields extending back to at least 120°. We also see the effect of the wake on the surface potential (Figure 1b): as density decreases and electron temperature increases with angle, the surface potential also becomes increasingly negative (<−200 V at 120° and to −500 V on the lunar antisolar point). One other point in examining Figure 1e: we note that $|E_z| \gg |E_x|$ which drives like-charged grain trajectories in the vertical direction. There is no evidence of sheath-created near-surface horizontal E-fields that are comparable to the vertical E values. However, we also assume that the Moon is a smooth sphere with no topographic features. In this case, the E-field is directed along the surface normal and intensifies in regions where solar wind electron currents are blocked. We will consider varied topography in the next section.

[11] We conclude that in a plasma wake, the plasma densities become low, electron temperature becomes high, and this combination gives rise to large local near-surface E-fields nearly aligned with the surface normal. Figure 1 shows a fluid model of wake with neutrality ($n_e = n_i$) imposed. However, kinetic models of the plasma expansion behind the Moon [*Ogilvie et al.*, 1996; *Farrell et al.*, 1998; *Birch and Chapman*, 2001; *Borisov and Mall*, 2006] indicate that the high-speed thermal electrons migrate into the wake ahead of the slower, massive ions, creating an ambipolar E-field and a distinct absence of ions in near-terminator wake plasma (i.e., $n_e \gg n_i$). This non-neutral ambipolar effect has not been included here, but will tend to make the ratio J_e/J_i even greater than that currently modeled in the wake region, effectively making the surface potential even more negative than shown in Figure 1b.

[12] Given the E-field structure shown in Figure 1a, a set of test dust grains were placed in the simulated field to

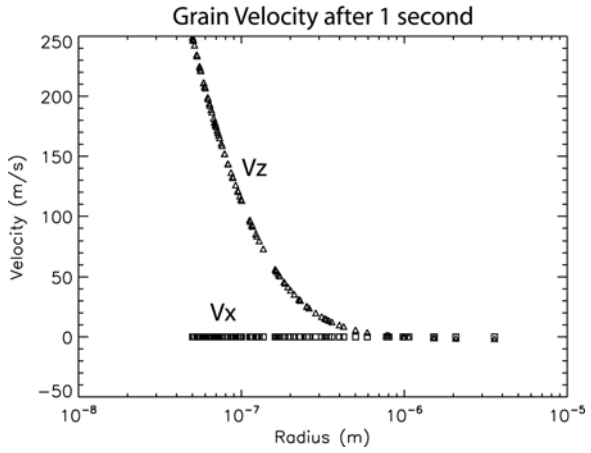

Figure 2. The grain velocity as a function of radius after repulsion from the surface at a location of 97.5° from the subsolar point. Note that the vertical velocities greatly exceed the horizontal velocities for smaller grains.

determine their acceleration after 1 second. No surface cohesion was assumed, and the particles felt the full force of the E-field. The location of the test particles is at 97.5° (7.5° from the terminator) in a region of strong E-fields. The grains are assumed to be completely charged by the local plasma, with charging as $q = 4\pi\varepsilon_o r\varphi$, where r is the grain radius and φ is the local surface potential.

[13] Figure 2 shows the vertical and horizontal grain velocities after 1 second of acceleration in the local field. Note that larger grains (>0.5 μm) have low or no velocity. In contrast, smaller grains (<0.5 μm) are accelerated >100 m/sec in the vertical direction and are the grains identified by *Stubbs et al.* [2006] to be lofted to great heights (~100 km) above the surface. While grains of 0.1 μm (~10^{-17} kg) are accelerated up to many hundreds of kilometers per second in these large fields, we note that the direction of grain movement is primarily vertical (along the surface normal)–the ratio of $v_x/v_z \ll 1$ since the force components scale as $E_x|/|E_z| < 10^{-4}$.

4. Horizontal Grain Motion

[14] In order to have horizontal nightside moving grain motion like that detected by LEAM [*Berg et al.*, 1976], there must be the presence of some physical process imparting horizontal momentum to the grains. Micrometeoroid impact was considered, but this mechanism cannot account for the predominantly nightside-directed grain flow found at both terminators. Hence, a second possible way to obtain horizontal nightside grain flow is from local solar wind "orographic" effects near the Apollo 17 landing area in the Taurus-Littrow valley where LEAM is deployed. The wake modeled in Figure 1 applies to the case of a smooth lunar surface near the terminator. The obstruction of solar wind occurs on the dayside creating a plasma void/wake on the nightside. However, if the local terrain varies on scale sizes larger than the Debye length (10's of meters), then local obstruction of the solar wind (an orographic effect) will occur near mountains and craters creating local low density pockets—local wakes—leeward of the obstructing features. Such may be the case in the Apollo 17 landing area.

[15] *Berg* [1978] initially considered the possibility that partially-lit craters and mountain valleys (like those at sunrise/sunset) have complicated local potentials. Elevated regions would be sunlit positively charged and floor regions would be unlit negatively charge. This local potential difference would then lead to grains hopping from top to floor (and vice versa) with clear horizontal trajectories, as illustrated by *Berg*'s [1978] Figures 1 and 3. While this scenario would certainly lead to a difference in potential and horizontal grain motion, we suggest that this effect is greatly enhanced by the creation of local solar wind void/wake effects within the local crater/valley floor, this creating a large density depletion and, via analogy to Figure 1, producing a large negative surface potential on the antisunward/leeward facing side of the obstruction.

[16] The situation is illustrated in Figure 3. At local dawn (terminator crossing), the mountain tops are charged positive via photoemission processes, but shadowed valley floors are charged negative. However, at sunrise/sunset, the local solar wind flow is nearly tangent to the surface, and local solar wind "orographic" effects would create a low density plasma void region within the valley, as illustrated in Figure 3. Due to ambipolar effects [*Ogilvie et al.*, 1996; *Farrell et al.*, 1998], the solar wind plasma does eventually migrate into the void downstream from the obstruction, but the leeward side of the obstruction will develop a strong density depletion (void) trailing immediately behind the feature. Because of the low density and increased electron temperature in the depletion, the leeward surface of the obstruction becomes strongly negatively charged (like >90° in Figure 1) and has large E-fields that eject like-charged grains from its surface (along the surface normal). These grains will obtain high velocities like that shown in Figure 2, but now with a horizontal velocity component directed nightside, away from the negatively-charged surface (just as observed by *Berg et al.* [1976]).

[17] Figure 4 shows that Apollo 17 was in fact in a valley floor, surrounded by larger mountain regions located at 5–10 kilometers distance from the landing site. At local sunrise/sunset, these mountains would block solar wind creating a local plasma depletion and large E-fields on

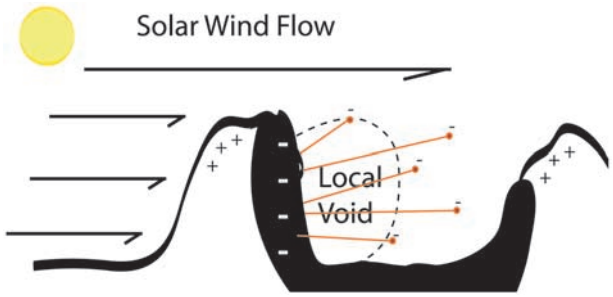

Figure 3. An illustration of local grain acceleration (red dots) due to topographic obstruction of the solar wind near the lunar terminator. A local plasma void forms on the face opposite the solar wind flow and large negative E-fields form at the surface. Like-charged grains would then be ejected from the surface.

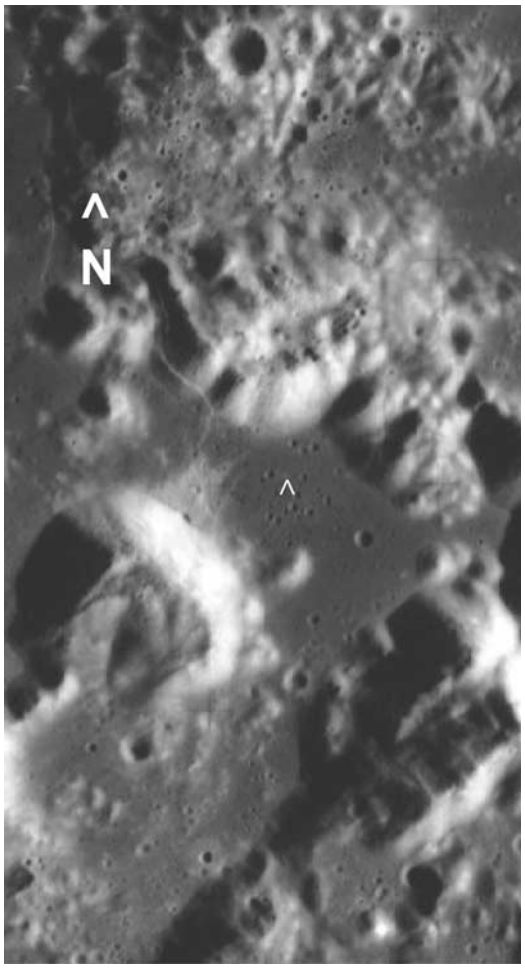

Figure 4. The Taurus-Littrow valley where Apollo 17's LEAM experiment landed. Note that mountains mostly surround the sensor (NASA image).

leeward mountain faces. Like-charged grains would then be lofted from such surfaces and measured by LEAM as nightside-flowing grains in the valley. We note that surrounding mountains both in the east and west guarantees that the effect will occur both at dawn and dusk terminator crossing, with predominant grain flow toward the nightside (westward at dawn, eastward at dusk) in both cases.

5. Conclusion

[18] We demonstrate that the E-fields increase substantially in locations immediately nightside of the terminator, in regions where there are no photoemission currents (i.e., no sunlight) and solar wind plasma currents are blocked by dayside portion of the lunar surface. By analogy, we also demonstrate that large E-fields are expected on the leeward side of large lunar features that are obstacles in the solar wind flow (e.g., mountains, crater rims). These local E-fields can then accelerate negative dust grains to large velocities. The fast-moving charged dust, directed towards the nightside, is essentially a new current source that alleviates the excessive negative charge buildup on the leeward surface and (partially) offsets the loss of electron flux in the now-obstructed solar wind. It is suggested that this process may account for the high-energy dust detected by Apollo 17's LEAM instrument [*Berg et al.*, 1976]. The planned lunar base at Shackleton crater is always near the terminator where we expect the frequent presence of accelerated dust. It is suggested to place landed packages like LEAM with plasma and E-field systems at various locations on the Moon (especially near Shackleton Crater) in order to better-characterize these fast moving grains and the effect of local topography on grain motion.

References

Berg, O. E. (1978), A lunar terminator configuration, *Earth Planet. Sci. Lett.*, *39*, 377.

Berg, O. E., et al. (1976). Lunar soil movement registered by the Apollo 17 cosmic dust experiment, in *Interplanetary Dust and Zodiacal Light*, edited by H. Elsasser et al., pp. 233–237, Springer, Berlin.

Birch, P. C., and S. C. Chapman (2001), Detailed structure and dynamics in particle-in-cell simulations of the lunar wake, *Phys. Plasmas*, *8*, 4551.

Borisov, N., and U. Mall (2006), Charging and motion of dust grains near the terminator of the Moon, *Planet. Space Sci.*, *54*, 572.

Farrell, W. M., M. L. Kaiser, J. T. Steinberg, and S. D. Bale (1998), A simple simulation of a plasma void: Applications to Wind observations of the lunar wake, *J. Geophys. Res.*, *103*, 23,653.

Halekas, J. S., S. D. Bale, D. L. Mitchell, and R. P. Lin (2005), Electrons and magnetic fields in the lunar plasma wake, *J. Geophys. Res.*, *110*, A07222, doi:10.1029/2004JA010991.

Manka, R. H. (1973), Plasma and potential at the lunar surface, in *Photon and Particle Interactions With Surfaces in Space*, edited by R. J. L. Grard, pp. 347–361, D., Reidel, Dordrecht, Netherlands.

McCoy, J. E., and D. R. Criswell (1974), Evidence for a high altitude distribution of lunar dust, *Proc. Lunar Sci. Conf.*, *5th*, 2991.

Ogilvie, K. W., J. T. Steinberg, R. J. Fitzenreiter, C. J. Owen, A. J. Lazarus, W. M. Farrell, and R. B. Torbert (1996), Observations of the lunar plasma wake from the WIND spacecraft on December 27, 1994, *Geophys. Res. Lett.*, *23*, 1255.

Samir, U., K. H. Wright Jr, and N. H. Stone (1983), The expansion of a plasma into a vacuum: Basic phenomena and processes and applications to space plasma physics, *Rev. Geophys.*, *21*, 1631.

Stubbs, T. J., et al. (2006), A dynamic fountain model for lunar dust, *Adv. Space Res.*, *37*, 59.

Stubbs, T. J., et al. (2007), Lunar surface charging: A global perspective using Lunar Prospector data, *Eur. Space Agency Spec. Publ.*, *ESA SP 643*, 181.

G. T. Delory and J. S. Halekas, Space Science Laboratory, University of California, Berkeley, 7 Gauss Way, Berkeley, CA 94720, USA.

W. M. Farrell and R. R. Vondrak, Solar System Exploration Division, NASA Goddard Space Flight Center, Code 690, Greenbelt, MD 20771, USA. (william.farrell@gsfc.nasa.gov)

T. J. Stubbs, Heliophysics Division, NASA Goddard Space Flight Center, Code 674, Greenbelt, MD 20771, USA.